Bacterial strain-dependent dissociation of cell recruitment and cell-to-cell spread in early *M. tuberculosis* infection

*B. Shoshana Zha[a,d], *Ludovic Desvignes[b], Tawania J. Fergus[b], Amber Cornelius[b], Tan-Yun Cheng[c], D. Branch Moody[c], and Joel D. Ernst[d]#

[a]Division of Pulmonary, Critical Care, Allergy and Sleep Medicine, Department of Medicine, University of California, San Francisco, California, USA

[b]Department of Medicine, New York University School of Medicine, New York, New York, USA

[c]Division of Rheumatology, Immunity and Inflammation, Department of Medicine, Brigham and Women's Hospital, Harvard Medical School, Boston, Massachusetts, USA

[d]Division of Experimental Medicine, Department of Medicine, University of California, San Francisco, California, USA

*Co-first authors; the order was determined by the leadership role in writing the paper

#Corresponding Author: Joel Ernst, MD

1001 Potrero Ave, Room 601

UCSF Box 1234

joel.ernst@ucsf.edu

Running title: *M. tuberculosis* dissemination and T cell priming

Keywords: Mycobacterium tuberculosis, Innate Response, T cell priming, Beijing strain

Word Count, Abstract: 139

Word Count, Text: 4,242

Abbreviations

Early secretory antigenic target secretion system (ESX), Mediastinal lymph node (MdLN), Mononuclear phagocyte (MNP), Monocyte-derived dendritic cells (moDC), Monocyte-derived recruited macrophages (RM), *Mycobacterium tuberculosis* (*M. tuberculosis*), neutrophils (neut), Phthiocerol dimycocerosates (PDIM), Phenolic glycolipids (PGL)

ABSTRACT

In the initial stage of respiratory infection, *Mycobacterium tuberculosis* traverses from alveolar macrophages to phenotypically diverse monocyte-derived phagocytes and neutrophils in the lung parenchyma. Here, we compare the *in vivo* kinetics of early bacterial growth and cell-to-cell spread of two strains of *M. tuberculosis*: a lineage 2 strain, 4334, and the widely studied lineage 4 strain H37Rv. Using flow cytometry, live cell sorting of phenotypic subsets, and quantitation of bacteria in cells of the distinct subsets, we found that 4334 induces less leukocyte influx into the lungs but demonstrates earlier population expansion and cell-to-cell spread. The earlier spread of 4334 to recruited cells, including monocyte-derived dendritic cells, is accompanied by earlier and greater magnitude of $CD4^+$ T cell activation. The results provide evidence that strain-specific differences in interactions with lung leukocytes can shape adaptive immune responses *in vivo*.

IMPORTANCE

Tuberculosis is a leading infectious disease killer world-wide and is caused by *Mycobacterium tuberculosis*. After exposure to *M. tuberculosis,* outcomes range from

apparent elimination to active disease. Early innate immune responses may contribute to differences in outcomes, yet it is not known how bacterial strains alter the early dynamics of innate immune and T cell responses. We infected mice with distinct strains of *M. tuberculosis* and discovered striking differences in innate cellular recruitment, cell-to-cell spread of bacteria in the lungs, and kinetics of initiation of antigen-specific CD4 T cell responses. We also found that *M. tuberculosis* can spread beyond alveolar macrophages even before a large influx of inflammatory cells. These results provide evidence that distinct strains of *M. tuberculosis* can exhibit differential kinetics in cell-to-cell spread which is not directly linked to early recruitment of phagocytes but is subsequently linked to adaptive immune responses.

INTRODUCTION

Mycobacterium tuberculosis is a facultative intracellular bacterium that resides in tissue mononuclear phagocytes (MNP) and granulocytes (1, 2). Previous investigations have shown that *M. tuberculosis* first enters alveolar macrophages (3, 4). After replication in alveolar macrophages, the bacteria subsequently spread to multiple subsets of phagocytes in the lung parenchyma, largely recruited from circulating monocytes (5–7). Subsequently, monocyte-derived lung dendritic cells (moDC) acquire the bacteria and transport them to draining lymph nodes (2), where they transfer antigens to lymph node resident dendritic cells that prime antigen-specific T cells (8, 9). After proliferating and differentiating, effector T cells traffic to the lungs and arrest progression of the infection (10). *M. tuberculosis* antigen-specific T cell responses require 14-17 days to develop after aerosol infection of mice with the commonly-used H37Rv strain (2, 10), and an average of 6 weeks is required for development of

70 adaptive immune responses after infection in humans (11, 12). Considerable evidence
71 indicates that the rate-limiting step in initiating *M. tuberculosis* antigen-specific CD4 T
72 cell responses is acquisition of the bacteria by dendritic cells in the lung, and transport
73 of live bacteria to local draining lymph nodes (8, 10, 13–16).

74 The mechanisms of cell-to-cell spread of *M. tuberculosis* are incompletely
75 understood, although evidence suggests a role for necrosis of infected cells and release
76 of viable bacteria that are subsequently ingested by other cells (17). Virulent strains of
77 *M. tuberculosis* can inhibit apoptosis (18) through multiple mechanisms including
78 upregulation of the antiapoptotic protein Mcl-1 (19), inhibition of NOX2-induced reactive
79 oxygen species formation (20), upregulation of soluble TNF receptor 2 (21), and
80 inhibition of apoptotic envelope stabilization (22), although induction of apoptosis still
81 occurs and is important for control of *M. tuberculosis in vivo* (23). Conversely, virulent
82 *M. tuberculosis* can promote necrosis through mitochondrial transmembrane potential
83 disruption (24), depletion of host cellular NAD^+ (25), and inhibition of plasma membrane
84 repair with induction of lipoxin A4 (17, 26), among other mechanisms.

85 The early secretory antigenic target secretion system (ESX)-1, a type VII
86 secretion system encoded by the RD1 locus of *M. tuberculosis* (27, 28), is implicated in
87 multiple mechanisms for its role in *M. tuberculosis* virulence (29–32). These
88 mechanisms include recruitment of macrophages (33), activation of neutrophils (34),
89 and secretion of immunodominant T cell antigens (ESAT-6 and CFP-10) (35–37). In
90 addition, ESX-1 has been linked to induction of macrophage necrosis (38–40). ESX-1's
91 role in cellular recruitment and induction of cell death leads to the hypothesis that it
92 plays a key role in *M. tuberculosis* cell-to-cell transfer.

The majority of studies of early innate responses and bacterial cell-to-cell transfer focus on *M. tuberculosis* lineage 4 strains, especially H37Rv or Erdman. However, there are 6 other human-adapted lineages (41) which vary genetically, phenotypically, and degree of induction of inflammatory responses *in vitro* (42). Lineage 2, which includes the Beijing family, is thought to have enhanced pathogenicity (i.e. ability to cause disease) and less protection by BCG vaccination (43, 44). The Beijing family is defined by region of difference (RD) 105, and has 5 sublineages (45). Sublineage 207 has demonstrated increased pathogenicity in guinea pigs, and the strain 4334 within this sublineage was the source of more secondary cases of TB than any other in San Francisco, California (45).

Increasing evidence indicates that distinct *M. tuberculosis* strains exhibit differential interactions with innate immune responses, as reflected by differences in cytokine release (46, 47) and monocyte activation (48). The goal of this work was to characterize the kinetics of *M. tuberculosis* growth and cell-to-cell spread early in infection, to compare the results between two distinct strains of *M. tuberculosis*, and to assess the relationship of cell recruitment and bacterial spread to initiation of CD4 T cell responses. We found that H37Rv and 4334 differ in their recruitment of leukocytes to the lungs, spread from alveolar macrophages to other leukocytes, and the kinetics of antigen-specific CD4 T cell activation. Our work demonstrates strain dependent dissociation of inflammatory cell recruitment and bacterial cell-to-cell spread, and that the timing of cell-to-cell spread impacts the dynamics of antigen-specific CD4 T cell responses.

RESULTS

Differential early cell dynamics after aerosol infection with* M. tuberculosis *strains H37Rv, 4334, and H37Rv∆RD1.

To test the hypothesis that distinct *M. tuberculosis* strains vary in their initial interactions with the host, we quantitated live bacteria in the lungs of mice infected with H37Rv, 4334, or H37Rv lacking the virulence locus RD1 (H37Rv∆RD1) which encodes the ESX-1 type VII secretion system (27, 28) implicated in cell recruitment and inflammation (29, 30, 33, 37). Mice were infected via aerosol with 200-300 colony forming units (CFU) of each bacterial strain and analyzed at frequent time points 1-14 days post-infection, a short time frame that is known to be prior to development of detectable T cell responses. H37Rv exhibited a lag of approximately 72h in which the number of bacteria did not increase in the lungs, similar to that reported in other studies (49, 50). In contrast, strain 4334 grew without a similar lag, and exhibited an increase in the lung bacterial burden that was already detectable by day 3 (Fig. 1A). After day 6, the populations of both strains expanded steadily during the first 2 weeks of infection and were equivalent by day 10 post-infection. In contrast to the two ESX-1-replete strains, H37Rv∆RD1 experienced a prolonged lag in expansion (28). The three strains also differed in their induction of increased lung cellularity: H37Rv induced the most marked increases in cellularity; 4334 responses were intermediate; and H37Rv∆RD1 induced no detectable changes in the number of lung cells in the initial 14 days of infection (Fig. 1B).

We next compared and characterized the cell populations in the lungs during the first two weeks of infection with the three *M. tuberculosis* strains. For this, we used established cell phenotypic markers and flow cytometry to differentiate subsets in the

139 $CD45^{+}$ cell population: $CD11b^{neg/lo}CD11c^{pos}$ alveolar macrophages; $CD11b^{pos}CD11c^{pos}$
140 which includes moDC; Gr-$1^{hi}CD11c^{neg}$ neutrophils; Gr-$1^{int}CD11c^{neg}$ monocytes; and Gr-
141 $1^{neg}CD11c^{neg}$ monocyte-derived recruited macrophages (RM) (Fig. S1) (6). As shown in
142 Figure 2A, $CD11b^{neg/lo}CD11c^{pos}$ alveolar macrophages and $CD11b^{pos}CD11c^{pos}$ moDC
143 varied little during the first two weeks and did not differ in lungs of mice infected with
144 4334 or H37Rv. While Gr-$1^{hi}CD11c^{neg}$ neutrophils did not increase in the lungs during
145 the first two weeks of infection with any strain, numbers were consistently lower in the
146 lungs of mice infected with 4334 and H37RvΔRD1 than with H37Rv. The most striking
147 difference between strains was in Gr-$1^{int}CD11c^{neg}$ monocytes and Gr-$1^{neg}CD11c^{neg}$ RM.
148 As previously reported (2), mice infected with H37Rv showed a progressive increase in
149 Gr-$1^{int}CD11c^{neg}$ monocytes and Gr-$1^{neg}CD11c^{neg}$ RM in the lungs over the first two
150 weeks, while neither population increased significantly in lungs of mice infected with
151 4334 or H37RvΔRD1. These findings indicate that the initial cellular inflammatory
152 response to infection with virulent *M. tuberculosis* varies considerably when distinct
153 bacterial strains infect genetically homogeneous hosts.

154 **Mycobacterium tuberculosis *strain-dependent dynamics of spread to recruited***
155 ***lung cells.***

156 To compare the spread of H37Rv and 4334 from alveolar macrophages to
157 recruited inflammatory cells during the initial phase of infection, we used BSL3-
158 contained flow cytometry sorting of live cells belonging to the previously-identified lung
159 leukocyte subsets (2, 5, 8). We sorted the individual cell populations from infected lungs
160 at frequent intervals and plated the resulting sorted cell fractions on solid media for
161 bacterial quantitation. Consistent with recently-published results generated by flow

cytometry detection of cells that harbored fluorescent protein-expressing *M. tuberculosis* (3, 4), we found live bacteria exclusively in alveolar macrophages for the first days post-infection (Fig. 2B, Fig. S2B). On day 6 post-infection, live *M. tuberculosis* were detectable in Gr-1^{hi}CD11c^{neg} neutrophils in 2 of the 10 mice infected with strain 4334, but in none of the 15 mice infected with H37Rv, and the average number of live bacteria per cell remained higher in 4334 compared to H37Rv over time (Fig. S2A). Similarly, on day 8 post-infection, 2 of the 10 mice in the group infected with 4334 and none of the 15 infected with H37Rv had detectable live *M. tuberculosis* in Gr-1^{int}CD11c^{neg} monocytes, again with higher average number of live bacteria per cell until day 14. Within CD11b^{pos}CD11c^{pos} moDC, a significantly higher number of live *M. tuberculosis* were detected for strain 4334 than H37Rv at 8 days post-infection, but the average number of live bacteria per cell in 4334 was higher than H37Rv only until day 10. In Gr-1^{neg}CD11c^{neg} RM, the number of live *M. tuberculosis* per cell was not significantly different between the two strains, although the number of live bacteria per cell was slightly (but not statistically significantly) higher in 4334 than H37Rv at days 10 and 14 post infection.

H37RvΔRD1 expanded in alveolar macrophages at a rate similar to wild-type H37Rv between days 1 and 10. H37RvΔRD1 also spread to CD11b^{pos}CD11c^{pos} moDC and Gr-1^{hi}CD11c^{neg} neutrophils in quantities comparable to that of wild-type H37Rv by day 10. However, H37RvΔRD1 did not expand further between days 10 and 14. Of note, live H37RvΔRD1 was recoverable in only 2 out of 5 mice in Gr-1^{int}CD11c^{neg} monocytes at day 14, and one mouse out of 5 at day 8 in Gr-1^{neg}CD11c^{neg} RM.

One known difference with functional importance between *M. tuberculosis* isolates is the presence or absence of phenolic glycolipids (PGL), which are cell wall lipids that modulate virulence (51). PGLs have been implicated in macrophage recruitment (52), dendritic cell uptake, and reduction in inflammatory pathways (53). PGLs are absent from H37Rv and many clinical isolates but are expressed in HN878, a prototypical strain used to study the Beijing family. As 4334 is a member of the Beijing family (44), we determined if 4334 has PGLs. Using electrospray ionization-quadrupole time-of-flight-mass spectrometry (ESI-QTOF-MS), there was no detectable PGL in either 4334 and H37Rv (Fig. 3A,B) under conditions in which PGL was detected in HN878, and the structurally related long chain polyketide phthiocerol dimycocerosates (PDIM) was ionized and detected. This result excludes PGL production as the cause of differential cell-to-cell transfer in these two strains.

***Mycobacterium tuberculosis* 4334 is associated with less alveolar macrophage death than H37Rv.**

Considering the absence of a lag and immediate expansion of 4334 in alveolar macrophages *in vivo*, we examined the intracellular growth dynamics of 4334 and H37Rv. We infected *ex vivo* murine alveolar macrophages with 4334 or H37Rv at an MOI of 1, and quantitated CFU at 48 and 72h post-infection. In cultured alveolar macrophages, H37Rv did not expand compared with the input by 48h but expanded approximately 5-fold by 72h. In contrast, 4334 expanded 4-fold by 48h, and nearly 10-fold by 72h (Fig. 4A). These growth kinetics mimic the initial phase of infection *in vivo*, in which there was a delay in growth of H37Rv for the first 3 days while 4334 expanded without a similar lag (Fig. 1B).

207 To determine if the apparent difference in growth of 4334 and H37Rv in alveolar
208 macrophages was due to differential cell death, we quantitated infection, early
209 apoptosis, and late cell death 48h post-infection. Using *M. tuberculosis* strains
210 expressing DsRed fluorescent protein and flow cytometry, we observed a higher
211 frequency of infection in cultured alveolar macrophages by 4334 than H37Rv (Fig.
212 4B,C), consistent with the results obtained by CFU plating. We used a viability marker
213 (Zombie Aqua, ZA) and a phosphatidylserine-binding marker (Annexin V, AV) to
214 quantitate the viability of alveolar macrophages infected *ex vivo* (Fig. 4B). In this
215 scheme, ZA^-/AV^- cells are viable, ZA^-/AV^+ cells are considered apoptotic, ZA^+/AV^- are
216 necrotic, and ZA^+/AV^+ represent late death, regardless of the mode of death (54). We
217 found significantly less cell death in alveolar macrophages infected by either strain
218 compared to uninfected controls, with quantitatively lower rates of cell death with 4334
219 compared to H37Rv. Moreover, infection with strain 4334 was associated with a lower
220 frequency of apoptotic cells than H37Rv (Fig. 4D). There was no significant difference in
221 apoptosis or late death between the two strains in bystander cells (that are defined as
222 cells in the same well but lacking DsRed-expressing bacteria).

223 Cell-to-cell spread of *M. tuberculosis* is thought to involve bacteria released by
224 dying cells. However, our results indicate that 4334 spreads more efficiently despite
225 being associated with lower rates of death of alveolar macrophages. We therefore
226 sought alternative explanations for the early spread of 4334. Since the ESX-1 type VII
227 secretion system has also been implicated in cell-to-cell spread of *M. tuberculosis*, we
228 used liquid chromatography-mass spectrometry (LC-MS/MS) to analyze culture filtrate
229 (i.e. secreted) proteins of 4334 and H37Rv. This revealed significantly higher levels of 3

ESX-1 substrates (EspA, EspB, EspF) and relative higher levels of 3 additional substrates (EspC, ESAT-6, CFP-10) in culture filtrates of 4334 compared with H37Rv (Fig. S3). In contrast, proteins secreted by non-ESX mechanisms (Ag85B and Ag85C) did not differ between the two strains. The finding that cell-to-cell spread of *M. tuberculosis* is associated with quantitative ESX-1 activity and not with the frequency of cell death suggests an alternative mechanism of cell-cell spread and dissemination of *M. tuberculosis* independent of cell death.

Mycobacterium tuberculosis *strain-dependent dynamics of antigen-specific CD4 T cell priming.*

M. tuberculosis induction of antigen-specific CD4 T cell responses requires transport of live bacteria by migratory moDC from the lungs to the mediastinal draining lymph node (8, 10, 13). Since we found more live bacteria in $CD11b^{pos}CD11c^{pos}$ moDC from mice infected with 4334 than H37Rv as early as day 8 post-infection (Fig. 2B), we hypothesized that this could result in earlier antigen-specific CD4 T cell priming in the lung-draining lymph node. We first quantitated live bacteria in the mediastinal lymph node (MdLN) on day 14 post-infection, corresponding to the onset of antigen-specific CD4 T cell priming (10). This revealed approximately 3-fold more 4334 than H37Rv in the lymph node (Fig 5A). We have previously established that a threshold number of bacteria are required in the MdLN for priming of *M. tuberculosis* antigen-specific CD4 T cells (10), and therefore hypothesized that 4334 might activate an earlier CD4 T cell response than H37Rv. To test this, we adoptively transferred *M. tuberculosis* Ag85B-specific TCR transgenic (P25TCR-Tg) naïve CD4 T cells (labeled with CellTrace Violet) into mice 24h prior to aerosol infection. Examination of the adoptively transferred T cells

253 isolated from the MdLN revealed no proliferation at day 10 post-infection in mice
254 infected with either strain. In contrast, by day 14 post-infection, P25TCR-Tg CD4 T cells
255 had proliferated and expanded in mediastinal lymph nodes of mice infected with strain
256 4334 but not H37Rv (Fig. 5B-C). At day 17, P25TCR-Tg CD4 T cells had also
257 proliferated in mice infected with H37Rv, although at significantly lower frequency than
258 in mice infected with 4334.

259 IFNγ is essential for control of *M. tuberculosis* (55, 56). Therefore, we analyzed
260 both total IFNγ concentrations and CD4 T cell specific IFNγ production in the lungs of
261 infected mice of both strains. We found total IFNγ concentrations in lung homogenate
262 supernatants to be significantly higher in mice infected with 4334 than H37Rv at day 14
263 post-infection (Fig. S4A). We next quantitated IFNγ-producing T cells in the lungs (Fig.
264 S4B) and found that both endogenous and P25TCR-Tg IFNγ-producing T cells were
265 more abundant in mice infected with 4334 than H37Rv at day 14 post-infection, though
266 the difference was not statistically significant. By day 17 post-infection, P25TCR-Tg but
267 not endogenous, IFNγ-producing T cells were significantly more abundant in mice
268 infected with 4334 than H37Rv (Fig. 5D). Together, these results indicate that *M.*
269 *tuberculosis* strain 4334 spreads to moDC and initiates antigen-specific CD4 T cell
270 responses earlier than does strain H37Rv. This earlier spread to dendritic cells and T
271 cell priming happens despite strain 4334 inducing fewer inflammatory cells to the lung
272 early in infection, and is associated with accelerated priming of antigen-specific CD4 T
273 cells.

274 We investigated whether the more robust and earlier T cell response correlated
275 into superior long-term control of infection. Indeed, at 7 weeks post-infection, we found

276 a half-log reduction in CFU recovery from the lungs of mice infected with *M. tuberculosis*
277 strain 4334 versus H37Rv (Fig. S5A). Interestingly, while total cell numbers in the lungs
278 of mice infected with *M. tuberculosis* strain 4334 were significantly lower than H37Rv
279 infected mice (Fig. 2B), by 7 weeks this was reversed (Fig. S5B), and the total number
280 of lymphocytes appears to account for the difference in cellularity (Fig. S5D). The
281 increased cellularity also correlates with more granuloma-like lesions in the lungs of
282 mice infected with 4334 (Fig. S5C, S5E), resembling the pathologic findings reported in
283 guinea pigs (44).

284 **DISCUSSION**

285 The early host responses to pulmonary infection with *M. tuberculosis* are
286 beginning to be clarified (3, 4), although studies to date have not examined the potential
287 impact of bacterial strain diversity. We analyzed early cellular responses in mice
288 infected by aerosol with 4334, a lineage 2 strain (44), and compared this to responses
289 to H37Rv, from lineage 4. Using flow sorting of live lung cells, we compared cell
290 populations, bacterial growth, and bacterial spread from alveolar macrophages to
291 recruited cells in the first 2 weeks of infection. We found that 4334 induces less
292 inflammatory cell recruitment than H37Rv, resembling that of H37Rv lacking the RD1
293 locus. However, 4334 spreads beyond alveolar macrophages earlier and is present in
294 greater abundance in monocytes, neutrophils, and moDC. This results in earlier
295 trafficking of bacteria to the mediastinal lymph node, and in turn, is accompanied by
296 earlier and greater magnitude activation of Ag85B-specific CD4 T cells.

297 Recent studies have confirmed that alveolar macrophages are the first cells
298 infected in the lungs by *M. tuberculosis*, a fact that had long been speculated (6) but

299 only recently demonstrated (3, 4). Alveolar macrophages are initially permissive to *M.*
300 *tuberculosis* replication (4), likely through their inability to mount a large inflammatory
301 response while leading to the upregulation of self-preserving Nrf2 pathways (4) and lipid
302 metabolism (57). We did not find a difference in total $CD11b^{neg/lo}CD11c^{hi}$ alveolar
303 macrophages cell numbers after infection. However, there is an earlier expansion of
304 4334 with significantly higher CFU 8 days post-infection than in H37Rv infected mice,
305 due to a lag in initial H37Rv growth *in vivo* (49, 50). Since alveolar macrophages were
306 the only infected cells during this initial phase, we hypothesized that the differential
307 expansion of the two strains could be due to differences in intracellular replication in
308 alveolar macrophages. We confirmed that 4334 replicates at a higher rate than H37Rv
309 in cultured alveolar macrophages, and this is accompanied by a lower rate of cell death.
310 By 2 weeks after infection, alveolar macrophages have been found to translocate
311 from the alveolar space to the lung interstitium (3), providing the opportunity for spread
312 of *M. tuberculosis* to other cells. Extending our previous work as well as that of others
313 (3–5, 8), we observed spread of both H37Rv and 4334 to monocyte-derived dendritic
314 cells and macrophages. Here, we found differential spread to the $CD11b^{pos}CD11c^{pos}$
315 population, with 4334 appearing in this population at a higher rate than H37Rv 8 days
316 post-infection. Notably, this cell population includes moDC (5, 6), and although a small
317 percentage of alveolar macrophages also express CD11b (58, 59) with potential
318 upregulation during inflammation and infection (3, 60), those cells have not been found
319 to migrate to lymphoid tissues. Nonetheless, with the combined findings of an earlier
320 and higher rate of spread to neutrophils and monocyte-derived cells in mice infected
321 with 4334 versus H37Rv, our data implies greater spread of 4334 from alveolar

322 macrophages to recruited cells in spite of inducing recruitment of fewer inflammatory
323 cells than H37Rv.

324 The determinants and mechanisms of *M. tuberculosis* cell-to-cell spread are not
325 well understood, especially *in vivo*, but likely depend on multiple factors including host
326 cell recruitment, intracellular bacterial growth, cellular release, and survival in
327 extracellular spaces. In this work, we found that while 4334, a lineage 2 strain with
328 increased pathogenicity in guinea pigs (44) and the ability to induce higher levels of type
329 I interferons (61), recruits significantly fewer monocytes and cells that differentiated from
330 monocytes but demonstrates superior growth and/or survival rates in the cells it does
331 infect compared to H37Rv. This suggests that progression of infection is not solely
332 determined by cellular recruitment but also by the rates of intracellular replication and
333 transfer between host cells. Differential growth dynamics between *M. tuberculosis*
334 strains has been shown in multiple primary cell types, including human monocytes (62),
335 human monocyte-derived macrophages (63), and murine bone marrow-derived
336 macrophages (64). We hypothesize that the permissiveness of alveolar macrophages
337 for *M. tuberculosis* growth in the initial stage of infection (4, 57) maximizes the
338 intracellular growth variations between strains.

339 Multiple mechanisms can determine the intracellular survival and growth of *M.*
340 *tuberculosis*. We focused on differential host cell death since this is thought to play a
341 key role in cell-to-cell spread. Death-receptor induced apoptosis (23) and subsequent
342 efferocytosis (65) are key host mechanisms for control of *M. tuberculosis*. As opposed
343 to avirulent strains lacking the operon RD1 and thus functional ESX-1 machinery,
344 virulent strains of *M. tuberculosis* have been found to inhibit apoptosis (18) and promote

345 necrosis (66) through multiple mechanisms. Necrosis is hypothesized to be the major
346 mode of host cell death for bacterial cell-cell spread, as it allows release of bacilli into
347 the extracellular space for phagocytosis by permissive host cells, rather than being
348 contained in apoptotic vesicles and killed through efferocytosis (17, 33, 67, 68). In
349 contrast to that model, we found that 4334 sustains alveolar macrophage *ex vivo*
350 survival to a greater extent than does H37Rv, yet 4334 spreads more readily to other
351 cells in the lungs.

352 ESX-1 is implicated in the induction of cell death through the action of secreted
353 proteins including ESAT-6 (40), which is concentration dependent. We have shown that
354 4334 secretes higher levels of ESX-1 substrates compared to H37Rv, but this is not
355 correlated with activation of cell death of infected alveolar macrophages *ex vivo*. One
356 hypothesis of these discordant findings is the limitation of using *ex vivo* infection
357 modeling, however, the significant protection of alveolar macrophage viability in 4334-
358 infected cells over H37Rv-infected cells argues against differential induction of cell
359 death as a means of cell-to-cell spread. Rather, these results are compatible with a
360 model in which nonlytic release contributes to cell-to-cell spread of *M. tuberculosis* in
361 the lungs (70). Nonlytic release has been demonstrated in *Dictyostelium* amoebae,
362 where *M. marinum* and *M. tuberculosis* egress via ejection rather than lysis of the
363 amoebae (71), and *in vivo* in zebrafish where nonlytic cell-to-cell transfer of *M. marinum*
364 has been observed (72). Furthermore, *M. tuberculosis* can grow extracellularly (73, 74),
365 adding an additional possibility that 4334 survives extracellularly more effectively than
366 H37Rv, allowing uptake by diverse phagocytic cells. Teasing these differenitals is of
367 essential importance to understand the mechanism of tuberculosis cell spread.

We also found significantly more live 4334 *M. tuberculosis* than H37Rv in the draining mediastinal lymph node 14 days post-infection. This correlates with the timing and speed of 4334 spread to moDC, which transport *M. tuberculosis* to the draining mediastinal lymph node (2, 9). Of note, we focused on $CD11b^{pos}CD11c^{pos}$ DCs in this study. During homeostasis, conventional DCs (cDCs) have been classified into two populations in mice: cDC-1 ($CD26^{+}CD11c^{+}CD103^{+}CD11b^{-}$) and cDC-2 ($CD26^{+}CD11b^{+}CD11c^{+}CD172a^{+}$) (75, 76). cDC-1 have been characterized as inducing CD8 T cell activation (77) while cDC-2 are implicated in CD4 T cell activation (78). In previous work, we found that cells resembling cDC-2 carry live *M. tuberculosis* to the draining mediastinal lymph node (2, 5), and cDC-1 do not appear to be significantly infected by *M. tuberculosis* in the first two weeks of infection (4). We have previously shown cDC-2-like cells are derived from monocytes (5), and therefore have termed this population moDC. However, $CD11b^{pos}CD11c^{pos}$ migratory DCs do not prime CD4 T cells efficiently during *M. tuberculosis* infection (9), and we and others have previously demonstrated that infected moDC transfer antigen to resident mediastinal lymph node DC that in turn activate T cells (8, 9). Here, we observe a significant increase of T cell activation at 17 days post-infection in mice infected with 4334 which correlates with a higher bacterial burden in the draining lymph node at day 14 post-infection. These findings are consistent with the finding of earlier spread of the bacteria to $CD11b^{pos}CD11c^{pos}$ moDC in the lungs, but do not indicate whether the greater magnitude of Ag85B-specific CD4 T cell activation in the lymph node is the consequence of more moDC presenting antigen, or more antigen presented per moDC.

390 Earlier T cell activation can lead to superior control of *M. tuberculosis* infection
391 (13). Here, we demonstrate that 4334 induces an earlier antigen-specific T cell
392 response which is associated with a reduction in CFU 7 weeks post-infection compared
393 to H37Rv infected mice. In addition, the quantitatively greater accumulation of
394 lymphocytes in the lungs of mice infected with 4334 is associated with an increased
395 number of inflammatory lesions in the lung at this time point.

396 A limitation of this work is the resolution of the flow sorting strategy. As the work
397 prioritized identification and characterization of the cell populations that harbor live *M.*
398 *tuberculosis* in the initial days after infection when the bacterial burdens are low, the
399 number of surface markers used for sorting and the resolution of certain cell subsets
400 was limited. Nevertheless, the resolution of the subsets was sufficient to allow tracking
401 of the spread of *M. tuberculosis* from alveolar macrophages to recruited inflammatory
402 cells over time. An additional limitation is that the genetic and molecular differences
403 between H37Rv and 4334 were not identified, although we do rule out the lineage 2
404 specific virulence lipid, PGL, as one potential difference. While both strains were
405 isolated from patients with pulmonary TB, H37Rv was initially isolated in 1905 (79), and
406 4334 was isolated in the mid-2000s (44). It is not known whether or how passage and
407 storage of the two strains has resulted in genotypic or phenotypic differences from the
408 original patient isolates. However, we do rule out the lineage 2 specific virulence lipid,
409 PGL, and comparative genetic analysis of these strains, as well as future work on the
410 recognized differences between lineage 2 and 4 strains can now be considered in light
411 of these detailed findings during early in vivo infection.

412 In conclusion, we found that *M. tuberculosis* strain-dependent differences in the
413 rate of spread from alveolar macrophages to recruited leukocytes in the lungs is
414 associated with lower rates of alveolar macrophage death and with a lower rate and
415 extent of initial leukocyte recruitment to the lungs. The finding that enhanced spread
416 from alveolar macrophages is associated with lower rates of alveolar macrophage cell
417 death suggests that nonlytic mechanisms are likely to contribute to cell-to-cell spread of
418 *M. tuberculosis* in vivo. The data also reveal that the strains examined differ in their
419 ESX-1- (type VII) but not SecA (type I)-mediated protein secretion activity, which
420 correlates with enhanced spread, suggesting that Esx-1 may contribute to nonlytic
421 spread of *M. tuberculosis* in the early stages of infection in the lungs. Understanding the
422 mechanisms underlying these findings will provide further insights into the virulence of
423 *M. tuberculosis*.

424 **METHODS**

425 **Mice and Care**

426 C57BL/6 mice were purchased from the Jackson Laboratory. P25 TCR Tg mice
427 whose CD4 T cells recognize peptide 25 (aa 240-254) of *M. tuberculosis* antigen 85B in
428 complex with mouse MHC II I-A^b (10, 80) were crossed in-house with congenic $CD45.1^+$
429 (B6.SJL-$Ptprc^a$ $Pepc^b$/BoyJ) and with $Rag1^{-/-}$ mice. For infections with *M. tuberculosis*,
430 mice were housed under barrier conditions in the ABSL-3 facility at the NYU School of
431 Medicine. All mice were between 8 and 12 weeks of age at the beginning of the
432 experiment, and mice of both sexes were used. Mice were euthanized by CO_2
433 asphyxiation followed by cervical dislocation. All experiments were performed with the
434 prior approval of the NYU Institutional Animal Care and Use Committee (IACUC).

435 **Cell isolation for *in vitro* and *in vivo* experiments**

436 Alveolar macrophages (AM) were harvested by bronchoalveolar lavage (81), and
437 purity confirmed through flow cytometry analysis with $CD11c^{+}CD11b^{-}$ cells (2) above
438 90% and autofluorescence (82). AM were cultured for up to 4 days in RPMI 1640 with
439 10% heat-inactivated FBS, 2mM L-glutamine, 1mM sodium pyruvate, 1x β-
440 mercaptoethanol (Gibco), 10 mM HEPES, 10ng/mL of recombinant murine granulocyte-
441 macrophage colony-stimulating factor (Peprotech), and 10 U/ml penicillin – 10 µg/ml
442 streptomycin that was washed out prior to infection.

443 P25 TCR Tg CD4 T cells were isolated from the secondary lymphoid organs of
444 P25TCR-Tg/CD45.1/$Rag1^{-/-}$ mice by magnetic cell sorting using anti-CD4 conjugated
445 microbeads and an AutoMACS Classic sorter (Miltenyi Biotec), according to the
446 manufacturer's recommendations.

447 ***Mycobacterium tuberculosis* strains, growth, and infections**

448 *M. tuberculosis* H37Rv was grown as previously described (83). 4334 was
449 obtained and maintained as previously described (61). Mice were infected via the
450 aerosol route, using an inhalation exposure system (Glas-Col) (2). The infectious dose
451 was quantitated on day 1 by plating whole lung homogenates from 3–5 mice on
452 Middlebrook 7H11 agar. To determine the bacterial load throughout the infection, lungs
453 were harvested, homogenized, and serial dilutions were plated on Middlebrook 7H11
454 agar. Colony Forming Units (CFUs) were counted after incubation of plates at 37°C for
455 3 weeks.

456 For *in vitro* infections, mycobacteria were grown to mid-log phase, pelleted at
457 3750 g, resuspended in PBS + 0.5% Tween 80, re-pelleted and excess Tween 80

458 washed off by centrifugation in PBS. The final pellet was re-suspended in RPMI 1640
459 with 10% serum, the bacterial density was evaluated by measuring absorbance at 580
460 nm, and the multiplicity of infection was adjusted to the mammalian cell density.

461 **Flow cytometry and cell sorting**

462 Lungs were removed and processed into single-cell suspensions for flow
463 cytometry and cell sorting as previously described (2, 84). Antibodies conjugated to
464 various fluorophores and directed against surface markers were:

Antibody	Clone	Source
B220-PE	RA3-6B2	BioLegend
CD4-BUV395	RM4-5	BD Biosciences
CD4-APC/Cy7	RM4-5	BioLegend
CD8-APC	53-6.7	BioLegend
CD8-BV421	53-6.7	BioLegend
CD11c-PerCP	HL3	BioLegend
CD11b-APC/Cy7	M1/70	BD Biosciences
CD19-FITC	6D5	BioLegend
CD45-PE	30-F11	BD Biosciences
CD45-FITC	30-F11	BD Biosciences
CD45.1-AF700	A20	BioLegend
CD45.2-PerCp/Cy5.5	104	BD Biosciences
CD45.2-FITC	104	BD Biosciences
CD90.2-PerCP/Cy5.5	30-H12	BioLegend
Gr-1-APC	RB6-8C5	BD Biosciences
Ly6C-FITC	AL-21	BD Biosciences
Ly6G-AF647	1A8	BioLegend
Siglec-F-PE	E50-2440	BD Biosciences

465 For flow cytometry analysis, stained samples were fixed overnight in 1%
466 paraformaldehyde. A minimum of 200,000 events per sample, gated on single cells
467 using forward and side scatter parameters, were acquired using an LSRII and
468 FACSDiva software (BD Biosciences).

469 For live cell sorting, fluorescently labeled live cells were acquired using a BSL3-
470 contained iCyt/Sony Synergy cell sorter. Cells were first separated in non-hematopoietic

471 cells ($CD45^-$), AM ($CD45^+CD11b^-CD11c^+$), monocyte-derived dendritic cells (moDC,
472 $CD45^+CD11b^+CD11c^+$) and other myeloid cells ($CD45^+CD11b^+CD11c^{neg/low}$). Then, this
473 latter fraction was re-acquired and sorted into neutrophils (Neut, $Gr1^{hi}CD11c^-$),
474 monocytes ($Gr1^{int}CD11c^-$) and recruited macrophages ($Gr\text{-}1^-CD11c^{low}$). All cell fractions
475 were collected and plated for CFU recovery and quantitation on agar as described
476 above. For flow cytometry and cell sorting, acquisition data were analyzed using FlowJo
477 software (TreeStar).

478 ***Mycobacterium tuberculosis*-antigen specific T cell adoptive transfer,**
479 **proliferation, and IFNγ stimulation**

480 P25TCR-Tg/CD45.1/$Rag1^{-/-}$ $CD4^+$ T cells were stained with CellTrace Violet
481 (ThermoFisher Scientific), according to the manufacturer's recommendations. Cells
482 were re-suspended at 2-3x10^6 cells/100 µl in sterile PBS for intravenous injection via
483 the retro-orbital route into anesthetized $CD45.2^+$ C57BL/6 recipient mice. Recipient mice
484 were infected with aerosolized *M. tuberculosis* 24h post-T cell transfer. T cell
485 proliferation was assessed at selected time points post-infection by quantitating
486 CellTrace Violet dilution by flow cytometry. Whole lung supernatants were analyzed for
487 IFNγ levels by ELISA.

488 **Quantification of Necrotic and Apoptotic Cells**

489 AM were infected with *M. tuberculosis* expressing DsRed for designated times,
490 after which cells were washed and then lifted with cold PBS containing 0.5 mM EDTA.
491 Cells were fixed, washed, and stained with Stain Zombie Aqua (Biolegend) to quantify
492 necrosis and AnnexinV-APC to quantify apoptosis (BD Biosciences) per manufacturer

493 protocols, washed with PBS, and analyzed by flow cytometry for DsRed (bacteria),
494 Annexin V, and Zombie Aqua.

495 **Analysis of PDIM and PGL**

496 Bacterial strains were grown shaking at 37°C for ~7 days to an OD580 of 0.6 in
497 Middlebrook 7H9 broth supplemented with 10% Oleic acid/dextrose/catalase and 0.05%
498 Tween 80. Cultures were centrifuged, supernatant removed, and pellets washed twice,
499 resuspended in 1mL of CH_3OH and contacted with 25mL $CHCl_3/CH_3OH$ (2:1) overnight.
500 Lipid was then extracted, dissolved in $CHCl_3$:CH_3OH at 1mg/mL, and ran on an Agilent
501 Technologies 6520 Accurate-Mass Q-Tof and 1200 series HPLC as previously
502 described (85).

503 **ESX-1 Secretion Assay**

504 Bacterial strains were grown shaking at 37°C for ~7 days in Middlebrook 7H9
505 broth supplemented with 10% Oleic acid/dextrose/catalase and 0.05% Tween 80 to an
506 OD580 0.4 – 0.7. Cultures were centrifuged, washed thrice in Sauton's media (0.5 g
507 KH2PO4, 0.5 g MgSO4, 4.0 g L-asparagine, 60 ml glycerol, 0.05 g Ferric ammonium
508 citrate, 2.0 g citric acid, 0.1 ml 1% ZnSO4, dH20 to 900 ml, 2.5 ml 20% Tween-80), and
509 incubated for an additional 24 hours. Bacteria were centrifuged at 2500 g for 10 min,
510 and supernatants passed through 0.2 µm syringe filters to obtain filtrates. Samples were
511 reconstituted in 200uL of 2M urea, reduced with DTT at 57°C for 1h, alkylated with 0.5M
512 iodacetamide for 45 min at RT, followed by trypsin digestion and cleansed as previously
513 described (86). After SpeedVac concentration, samples reconstituted in 0.5% acetic
514 acid, and loaded onto an Acclaim PepMap trap column in line with an EASY Spray
515 50cm x 75µm ID PepMap C18 analytical HPLC column with 2µm bead size using the

516 auto sampler of an EASY-nLC 1000 HPLC (ThermoFisher) and solvent A (2%
517 acetonitrile, 0.5% acetic acid). The peptides were gradient eluted into a Q Exactive
518 (Thermo Scientific) mass spectrometer using a 2h linear gradient from 2% to 40%
519 solvent B (95% acetonitrile, 0.5% acetic acid), followed by 10 min from 40% to 100%
520 solvent B. Solvent B was held at 100% for another 10 min for column wash. Spectra
521 were acquired using the following parameters: resolution of 70,000, an automatic gain
522 control of 1e6, with a maximum ion time of 120 ms, and scan range of 300 to 1500 m/z.
523 Following each full MS scan twenty data-dependent high resolution HCD MS/MS
524 spectra were acquired. All MS/MS spectra were collected using the following
525 instrument parameters: resolution of 17,500, AGC target of 2e5, maximum ion time of
526 250 ms, one microscan, 2 m/z isolation window, fixed first mass of 150 m/z, and
527 normalized collision energy of 27.

528 All acquired MS/MS spectra were searched against a combined database for
529 H37Rv and NITR203 on UniProt, using Andromeda search algorithm and MaxQuant for
530 quantitation (87). The data set was filtered to remove proteins with only one unique
531 peptide and that were not detected in all three replicates of at least one strain. LFQ
532 intensity values were $\log_2$ transformed. A two-sided t-test and correcting for multiple
533 testing by controlling for FDR at 5% using Benjamini-Hochberg's method. In addition, z-
534 scores were calculated and used to perform hierarchical clustering.

535 **Histopathology**

536 The left lung was excised, fixed in 10% buffered formalin for one week at room
537 temperature, then embedded in paraffin. 5 μm sections were cut and stained with
538 hematoxylin and eosin. Whole lung sections were scanned at 40X by the NYU School of

539 Medicine Experimental Pathology Research Laboratory, using a Leica SCN400 F
540 whole-slide scanner. Digital images were used for the quantitation of lung
541 histopathology using the open-source image processing software Fiji, with two
542 independent approaches. Briefly, the total surface area of the lung section was
543 calculated, then the contributions of airways and blood vessels to that area were
544 subtracted, leaving the contribution of the structural tissues. The proportion of
545 inflammatory infiltrates within those tissues was then quantitated, either by manual
546 contouring or using automated color density contouring. For each 40X section, the final
547 percentage of lung inflammatory infiltrate was calculated as the average of the values
548 obtained by each method.

549 **Statistical analysis**

550 Experiments were performed at least twice, with exception of experiments
551 focusing on H37RvΔRD1 and 7 weeks post-infection which were performed once.
552 Results are expressed as mean and standard deviation (SD). Unless otherwise stated,
553 parametric Student two-tailed t test and Holm multiple comparisons correction, with a
554 95% confidence interval was used to compare experimental groups, with $p<0.05$
555 considered significant.

556 **ACKNOWLEDGMENTS**

557 We thank Diane Ordway and Midori Kato-Maeda for the *M. tuberculosis* strain
558 4334. Cynthia Portal-Celhay and Thais Klevorn aided in experiments. We acknowledge
559 the expertise and support of Beatrix Ueberheide and Jessica Chapman-Lim at the NYU
560 Proteomics Laboratory, supported in part by NYU Langone Health and the Laura and
561 Isaac Perlmutter Cancer Center Support Grant P30CA016087 from the National Cancer

562 Institute, for proteomics assays. Cell sorting and flow cytometry were performed by
563 Michael Gregory from the NYU Cytometry and Cell Sorting Laboratory, which is
564 supported in part by grant P30CA016087 from the National Institutes of Health/National
565 Cancer Institute.

566 This project was supported by NIH grants R01 AI051242 and R01 AI049313, as
567 well as an award from the Stony Wold-Herbert Fund.

568 L.D. and J.D.E. designed the experiments, B.S.Z, L.D., and J.D.E. analyzed the
569 results; T.J.F., L.D., and A.C. conducted experiments; T.Y and D.B.M. provided the
570 lipidomic analysis and reviewed the manuscript; B.S.Z, L.D., and J.D.E. wrote the
571 manuscript.

572

573 **REFERENCES**

574 1. Sabin FR, Doan CA. 1927. The relation of monocytes and clasmatocytes to early
575 infection in rabbits with bovine tubercle bacilli. J Exp Med 46:627–644.

576 2. Wolf AJ, Linas B, Trevejo-Nuñez GJ, Kincaid E, Tamura T, Takatsu K, Ernst JD.
577 2007. Mycobacterium tuberculosis infects dendritic cells with high frequency and
578 impairs their function in vivo. J Immunol 179:2509–2519.

579 3. Cohen SB, Gern BH, Delahaye JL, Adams KN, Plumlee CR, Winkler JK, Sherman
580 DR, Gerner MY, Urdahl KB. 2018. Alveolar macrophages provide an early
581 Mycobacterium tuberculosis niche and initiate dissemination. Cell Host Microbe
582 24:439–446.

583 4. Rothchild AC, Olson GS, Nemeth J, Amon LM, Mai D, Gold ES, Diercks AH,
584 Aderem A. 2019. Alveolar Macrophages Generate a Noncanonical NRF2-Driven

585 Transcriptional Response to Mycobacterium tuberculosis in vivo. Sci Immunol
586 4:eaaw6693.
587 5. Norris BA, Ernst JD. 2018. Mononuclear cell dynamics in M. tuberculosis infection
588 provide opportunities for therapeutic intervention. PLoS Pathog 14:e1007154.
589 6. Srivastava S, Ernst JD, Desvignes L. 2014. Beyond macrophages: The diversity
590 of mononuclear cells in tuberculosis. Immunol Rev 262:179–192.
591 7. Skold M, Behar SM, Sköld M, Behar SM. 2014. Tuberculosis triggers a tissue-
592 dependent program of differentiation and acquisition of effector functions by
593 circulating monocytes. J Immunol 181:6349–6360.
594 8. Srivastava S, Ernst JD. 2014. Cell-to-cell transfer of M. tuberculosis antigens
595 optimizes CD4 T cell priming. Cell Host Microbe 15:741–752.
596 9. Samstein M, Schreiber HA, Leiner IM, Sušac B, Glickman MS, Pamer EG. 2013.
597 Essential yet limited role for CCR2+ inflammatory monocytes during
598 Mycobacterium tuberculosis-specific T cell priming. Elife 2:e01086.
599 10. Wolf AJ, Desvignes L, Linas B, Banaiee N, Tamura T, Takatsu K, Ernst JD. 2008.
600 Initiation of the adaptive immune response to Mycobacterium tuberculosis
601 depends on antigen production in the local lymph node, not the lungs. J Exp Med
602 205:105–115.
603 11. Poulsen A. 1950. Some clinical features of Tuberculosis. Acta Tuberc Scand
604 24:311–346.
605 12. Wallgren A. 1948. A time-table of Tuberculosis. Tubercle 29:245–251.
606 13. Chackerian AA, Alt JM, Perera T V, Dascher CC, Behar SM. 2002. Dissemination
607 of Mycobacterium tuberculosis is influenced by host factors and precedes the

608 initiation of T-cell immunity. Infect Immun 70:4501–4509.
609 14. Blomgran R, Ernst JD. 2011. Lung neutrophils facilitate activation of naïve
610 antigen-specific CD4+ T cells during Mycobacterium tuberculosis infection. J
611 Immunol 186:7110–7119.
612 15. Blomgran R, Desvignes L, Briken V, Ernst JD. 2012. Mycobacterium tuberculosis
613 inhibits neutrophil apoptosis, leading to delayed activation of naive CD4 T cells.
614 Cell Host Microbe 11:81–90.
615 16. Grace PS, Ernst JD. 2015. Suboptimal antigen presentation contributes to
616 virulence of Mycobacterium tuberculosis in vivo. J Immunol 196:357–364.
617 17. Divangahi M, Chen M, Gan H, Desjardins D, Hickman TT, Lee DM, Fortune S,
618 Behar SM, Remold HG. 2009. Mycobacterium tuberculosis evades macrophage
619 defenses by inhibiting plasma membrane repair. Nat Immunol 10:899–906.
620 18. Keane J, Remold HG, Kornfeld H. 2000. Virulent Mycobacterium tuberculosis
621 Strains Evade Apoptosis of Infected Alveolar Macrophages. J Immunol 164:2016–
622 2020.
623 19. Sly LM, Hingley-Wilson SM, Reiner NE, McMaster WR. 2003. Survival of
624 Mycobacterium tuberculosis in host macrophages involves resistance to
625 apoptosis dependent upon induction of antiapoptotic Bcl-2 family member Mcl-1. J
626 Immunol 170:430–437.
627 20. Briken V, Miller JL. 2008. Living on the edge: Inhibition of host cell apoptosis by
628 Mycobacterium tuberculosis. Future Microbiol 3:415–422.
629 21. Remold M Katarzyna Balcewicz-Sablinska HG, Keane J. 1998. Pathogenic
630 Mycobacterium tuberculosis evades apoptosis of host macrophages by release of

631 TNF-R2, resulting in inactivation of TNF-a. J Immunol 161:2636–2641.
632 22. Gan H, Lee J, Ren F, Chen M, Kornfeld H, Remold HG. 2008. Mycobacterium
633 tuberculosis blocks crosslinking of annexin-1 and apoptotic envelope formation on
634 infected macrophages to maintain virulence. Nat Immunol 9:1189–1197.
635 23. Stutz MD, Allison CC, Ojaimi S, Preston SP, Doerflinger M, Arandjelovic P,
636 Whitehead L, Bader SM, Batey D, Asselin-Labat M-L, Herold MJ, Strasser A,
637 West NP, Pellegrini M. 2021. Macrophage and neutrophil death programs
638 differentially confer resistance to tuberculosis. Immunity 54:1758–1771.
639 24. Chen M, Gan H, Remold HG. 2006. A mechanism of virulence: Virulent
640 Mycobacterium tuberculosis strain H37Rv, but not attenuated H37Ra, causes
641 significant mitochondrial inner membrane disruption in macrophages leading to
642 necrosis. J Immunol 176:3707–3716.
643 25. Sun J, Siroy A, Lokareddy RK, Speer A, Doornbos KS, Cingolani G, Niederweis
644 M. 2015. The tuberculosis necrotizing toxin kills macrophages by hydrolyzing
645 NAD. Nat Struct Mol Biol 22:672–678.
646 26. Chen M, Divangahi M, Gan H, Shin DSJ, Hong S, Lee DM, Serhan CN, Behar
647 SM, Remold HG. 2008. Lipid mediators in innate immunity against tuberculosis:
648 Opposing roles of PGE 2 and LXA 4 in the induction of macrophage death. J Exp
649 Med 205:2791–2801.
650 27. Stanley SA, Raghavan S, Hwang WW, Cox JS. 2003. Acute infection and
651 macrophage subversion by Mycobacterium tuberculosis require a specialized
652 secretion system. PNAS 100:13001–13006.
653 28. Pym AS, Brodin P, Brosch R, Huerre M, Cole ST. 2002. Loss of RD1 contributed

654 to the attenuation of the live tuberculosis vaccines Mycobacterium bovis BCG and
655 Mycobacterium microti. Mol Microbiol 46:709–717.
656 29. Koo IC, Wang C, Raghavan S, Morisaki JH, Cox JS, Brown EJ. 2008. ESX-1-
657 dependent cytolysis in lysosome secretion and inflammasome activation during
658 mycobacterial infection. Cell Microbiol 10:1866–1878.
659 30. Mishra BB, Moura-Alves P, Sonawane A, Hacohen N, Griffiths G, Moita LF, Anes
660 E, Moura-Alves P, Sonawane A, Hacohen N, Griffiths G, Moita LF, Anes E. 2010.
661 Mycobacterium tuberculosis protein ESAT-6 is a potent activator of the
662 NLRP3/ASC inflammasome. Cell Microbiol 12:1046–1063.
663 31. Wassermann R, Gulen MF, Sala C, Perin SG, Lou Y, Rybniker J, Schmid-Burgk
664 JL, Schmidt T, Hornung V, Cole ST, Ablasser A. 2015. Mycobacterium
665 tuberculosis differentially activates cGAS- and inflammasome-dependent
666 intracellular immune responses through ESX-1. Cell Host Microbe 17:799–810.
667 32. Conrad WH, Osman MM, Shanahan JK, Chu F, Takaki KK, Cameron J,
668 Hopkinson-Woolley D, Brosch R, Ramakrishnan L. 2017. Mycobacterial ESX-1
669 secretion system mediates host cell lysis through bacterium contact-dependent
670 gross membrane disruptions. PNAS 114:1371–1376.
671 33. Davis JM, Ramakrishnan L. 2009. The role of the granuloma in expansion and
672 dissemination of early Tuberculous infection. Cell 136:37–49.
673 34. Welin A, Björnsdottir H, Winther M, Christenson K, Oprea T, Karlsson A, Forsman
674 H, Dahlgren C, Bylund J. 2015. CFP-10 from Mycobacterium tuberculosis
675 selectively activates human neutrophils through a pertussis toxin-sensitive
676 chemotactic receptor. Infect Immun 83:205–213.

677 35. Brandt L, Oettinger T, Holm A, Andersen AB, Anderson P, Andersen P. 1996. Key
678 epitopes on the ESAT-6 antigen recognized in mice during the recall of protective
679 immunity to Mycobacterium tuberculosis. J Immunol 157:3527–33.
680 36. Elhay MJ, Oettinger T, Andersen P. 1998. Delayed-type hypersensitivity
681 responses to ESAT-6 and MPT64 from Mycobacterium tuberculosis in the guinea
682 pig. Infect Immun 66:3454–3456.
683 37. Ravn P, Demissie A, Eguale T, Wondwosson H, Lein D, Amoudy HA, Mustafa
684 AS, Kok Jensen A, Holm A, Rosenkrands I, Oftung F, Olobo J, von Reyn F,
685 Andersen P. 1999. Human T cell responses to the ESAT-6 antigen from
686 Mycobacterium tuberculosis. J Infect Dis 179:637–645.
687 38. Wong KW, Jacobs WR. 2011. Critical role for NLRP3 in necrotic death triggered
688 by Mycobacterium tuberculosis. Cell Microbiol 13:1371–1384.
689 39. Dallenga T, Repnik U, Corleis B, Eich J, Reimer R, Griffiths GW, Schaible UE.
690 2017. M. tuberculosis-induced necrosis of infected neutrophils promotes bacterial
691 growth following phagocytosis by macrophages. Cell Host Microbe 22:519–530.
692 40. Francis RJ, Butler RE, Stewart GR. 2014. Mycobacterium tuberculosis ESAT-6 is
693 a leukocidin causing Ca2+ influx, necrosis and neutrophil extracellular trap
694 formation. Cell Death Dis 5:e1474.
695 41. Brites D, Gagneux S. 2017. The nature and evolution of genomic diversity in the
696 Mycobacterium tuberculosis vomplex. Adv Exp Med Biol 1019:1–26.
697 42. Coscolla M, Gagneux S. 2014. Consequences of genomic diversity in
698 mycobacterium tuberculosis. Semin Immunol 26:431–444.
699 43. Kremer K, Van Der Werf MJ, Au BKY, Anh DD, Kam KM, Van Doorn HR,

700 Borgdorff MW, Van Soolingen D. 2009. Vaccine-induced immunity by typical
701 Mycobacterium tuberculosis Beijing strains. Emerg Infect Dis 15:335–339.
702 44. Kato-Maeda M, Shanley CA, Ackart D, Jarlsberg LG, Shang S, Obregon-Henao
703 A, Harton M, Basaraba RJ, Henao-Tamayo M, Barrozo JC, Rose J, Kawamura
704 LM, Coscolla M, Fofanov VY, Koshinsky H, Gagneux S, Hopewell PC, Ordway
705 DJ, Orme IM. 2012. Beijing sublineages of Mycobacterium tuberculosis differ in
706 pathogenicity in the guinea pig. Clin Vaccine Immunol 19:1222–1227.
707 45. Kato-Maeda M, Kim EY, Flores L, Jarlsberg LG, Osmond D, Hopewell PC. 2010.
708 Differences among sublineages of the East-Asian lineage of Mycobacterium
709 tuberculosis in genotypic clustering. Int J Tuberc Lung Dis 14:538–544.
710 46. Reiling N, Homolka S, Walter K, Brandenburg J, Niwinski L, Ernst M, Herzmann
711 C, Lange C, Diel R, Ehlers S, Niemann S. 2013. Clade-specific virulence patterns
712 of Mycobacterium tuberculosis complex strains in human primary macrophages
713 and aerogenically infected mice. MBio 4:e00250-13.
714 47. Portevin D, Gagneux S, Comas I, Young D. 2011. Human macrophage responses
715 to clinical isolates from the Mycobacterium tuberculosis complex discriminate
716 between ancient and modern lineages. PLoS Pathog 7:e1001307.
717 48. Manca C, Reed MB, Freeman S, Mathema B, Kreiswirth B, Barry CE, Kaplan G.
718 2004. Differential monocyte activation underlies strain-specific Mycobacterium
719 tuberculosis pathogenesis. Infect Immun 72:5511–5514.
720 49. Dietrich J, Roy S, Rosenkrands I, Lindenstrøm T, Filskov J, Rasmussen EM,
721 Cassidy J, Andersen P. 2015. Differential influence of nutrient-starved
722 Mycobacterium tuberculosis on adaptive immunity results in progressive

723 tuberculosis disease and pathology. Infect Immun 83:4731–4739.
724 50. Valdés I, Montoro E, Mata-Espinoza D, Asín O, Barrios-Payan J, Francisco-Cruz
725 A, Valdivia JA, Hernández-Pando R. 2014. Immunogenicity and protection
726 conferred by Mycobacterium habana in a murine model of pulmonary
727 tuberculosis. Tuberculosis 94:65–72.
728 51. Ly A, Liu J. 2020. Mycobacterial virulence factors: Surface-exposed lipids and
729 secreted proteins. Int J Mol Sci 21:3985.
730 52. Cambier CJ, Takaki KK, Larson RP, Hernandez RE, Tobin DM, Urdahl KB,
731 Cosma CL, Ramakrishnan L. 2014. Mycobacteria manipulate macrophage
732 recruitment through coordinated use of membrane lipids. Nature 505:218–222.
733 53. Tabouret G, Astarie-Dequeker C, Demangel C, Malaga W, Constant P, Ray A,
734 Honoré N, Bello NF, Perez E, Daffé M, Guilhot C. 2010. Mycobacterium leprae
735 Phenolglycolipid-1 Expressed by Engineered M. bovis BCG modulates early
736 interaction with human phagocytes. PLoS Pathog 6:e1001159.
737 54. Telford WG. 2018. Multiparametric analysis of apoptosis by flow cytometry, p.
738 167–202. *In* Methods in Molecular Biology. Humana Press Inc.
739 55. Flynn JL, Chan J, Triebold KJ, Dalton DK, Stewart TA, Bloom BR. 1993. An
740 essential role for Interferon-γ in resistance to Mycobacterium tuberculosis
741 infection. J Exp Med 173:2249–54.
742 56. Cooper AM, Dalton DK, Stewart TA, Griffin JP, Russell DG, Orme IM. 1993.
743 Disseminated Tuberculosis in Interferon 7 gene-disrupted mice. J Exp Med
744 178:2243–2247.
745 57. Huang L, Nazarova E V, Tan S, Liu Y, Russell DG. 2018. Growth of

746 Mycobacterium tuberculosis in vivo segregates with host macrophage metabolism
747 and ontogeny. J Exp Med 215:1135–1152.
748 58. Guth AM, Janssen WJ, Bosio CM, Crouch EC, Henson PM, Dow SW. 2009. Lung
749 environment determines unique phenotype of alveolar macrophages. Am J
750 Physiol Lung Cell Mol Physiol 296:936–946.
751 59. Lafuse WP, Rajaram MVS, Wu Q, Moliva JI, Torrelles JB, Turner J, Schlesinger
752 LS. 2019. Identification of an Increased Alveolar Macrophage Subpopulation in
753 Old Mice That Displays Unique Inflammatory Characteristics and Is Permissive to
754 Mycobacterium tuberculosis Infection . J Immunol 203:2252–2264.
755 60. Duan M, Steinfort DP, Smallwood D, Hew M, Chen W, Ernst M, Irving LB,
756 Anderson GP, Hibbs ML. 2016. CD11b immunophenotyping identifies
757 inflammatory profiles in the mouse and human lungs. Mucosal Immunol 9:550–
758 563.
759 61. Wiens KE, Ernst JD. 2016. The mechanism for Type I Interferon induction by
760 Mycobacterium tuberculosis is bacterial strain-dependent. PLoS Pathog
761 12:e1005809.
762 62. Li Q, Whalen CC, Albert JM, Larkin R, Zukowski L, Cave MD, Silver RF. 2002.
763 Differences in rate and variability of intracellular growth of a panel of
764 Mycobacterium tuberculosis clinical isolates within a human monocyte model.
765 Infect Immun 70:6489–6493.
766 63. Wu S, Howard ST, Lakey DL, Kipnis A, Samten B, Safi H, Gruppo V, Wizel B,
767 Shams H, Basaraba RJ, Orme IM, Barnes PF. 2004. The principal sigma factor
768 sigA mediates enhanced growth of Mycobacterium tuberculosis in vivo. Mol

769 Microbiol 51:1551–1562.
770 64. Park JS, Tamayo MH, Gonzalez-Juarrero M, Orme IM, Ordway DJ. 2006. Virulent
771 clinical isolates of Mycobacterium tuberculosis grow rapidly and induce cellular
772 necrosis but minimal apoptosis in murine macrophages. J Leukoc Biol 79:80–86.
773 65. Martin CJ, Booty MG, Rosebrock TR, Nunes-Alves C, Desjardins DM, Keren I,
774 Fortune SM, Remold HG, Behar SM. 2012. Efferocytosis is an innate antibacterial
775 mechanism. Cell Host Microbe 12:289–300.
776 66. Michelet X, Tuli A, Gan H, Geadas C, Sharma M, Remold HG, Brenner MB. 2018.
777 Lysosome-mediated plasma membrane repair is dependent on the small GTPase
778 Arl8b and determines cell death type in Mycobacterium tuberculosis infection. J
779 Immunol 200:3160–3169.
780 67. Mohareer K, Asalla S, Banerjee S. 2018. Cell death at the cross roads of host-
781 pathogen interaction in Mycobacterium tuberculosis infection. Tuberculosis
782 113:99–121.
783 68. Behar SM, Divangahi M, Remold HG. 2010. Evasion of innate immunity by
784 mycobacterium tuberculosis: Is death an exit strategy? Nat Rev Microbiol 8:668–
785 674.
786 69. Keane J, Remold HG, Kornfeld H. 2000. Virulent Mycobacterium tuberculosis
787 Strains Evade Apoptosis of Infected Alveolar Macrophages. J Immunol 164:2016–
788 2020.
789 70. Byrd TF, Green GM, Fowlston SE, Lyons CR. 1998. Differential growth
790 characteristics and streptomycin susceptibility of virulent and avirulent
791 Mycobacterium tuberculosis strains in a novel fibroblast-mycobacterium

792 microcolony assay. Infect Immun 66:5132–5139.
793 71. Hagedorn M, Ronde KH, Russell DG, Soldati T. 2009. Infection by tubercular
794 mycobacteria is spread by nonlytic ejection from their amoeba hosts. Science
795 323:1729–1733.
796 72. Cambier CJ, O'Leary SM, O'Sullivan MP, Keane J, Ramakrishnan L. 2017.
797 Phenolic glycolipid facilitates mycobacterial escape from microbicidal tissue-
798 resident macrophages. Immunity 47:552–565.
799 73. Woodruff CE. 1934. A free growth period of tubercle bacilli in the guinea pig
800 omentum as related to the hypersensitive state. Am J Pathol 10:739–756.
801 74. Rich A. 1944. The Pathogenesis of Tuberculosis, 1st ed. Charles C. Thomas,
802 Springfield, IL.
803 75. Bosteels C, Scott CL. 2020. Transcriptional regulation of DC fate specification.
804 Mol Immunol 121:38–46.
805 76. Guilliams M, Ginhoux F, Jakubzick C, Naik SH, Onai N, Schraml BU, Segura E,
806 Tussiwand R, Yona S. 2014. Dendritic cells, monocytes and macrophages: A
807 unified nomenclature based on ontogeny. Nat Rev Immunol 14:571–578.
808 77. Ng SL, Teo YJ, Setiagani YA, Karjalainen K, Ruedl C. 2018. Type 1 conventional
809 CD103+ dendritic cells control effector CD8+ T cell migration, survival, and
810 memory responses during influenza infection. Front Immunol 9:3043.
811 78. Dudziak D, Kamphorst AO, Heidkamp GF, Buchholz VR, Trumpfheller C,
812 Yamazaki S, Cheong C, Liu K, Lee H-W, Park CG, Steinman RM, Nussenzweig
813 MC. 2007. Differential antigen processing by dendritic cell subsets in vivo.
814 Science 315:107–111.

815 79. Steenken W, Gardner LU. 1946. HISTORY OF H37 STRAIN OF TUBERCLE
816 BACILLUS1. Am Rev Tuberc 54:62–66.
817 80. Tamura T, Ariga H, Kinashi T, Uehara S, Kikuchi T, Nakada M, Tokunaga T, Xu
818 W, Kariyone A, Saito T, Kitamura T, Maxwell G, Takaki S, Takatsu K. 2004. The
819 role of antigenic peptide in CD4+ T helper phenotype development in a T cell
820 receptor transgenic model. Int Immunol 16:1691–1699.
821 81. Rothchild A, Mai D, Aderem A, Diercks A. 2020. Flow cytometry analysis and
822 fluorescence-activated cell sorting of myeloid cells from lung and bronchoalveolar
823 lavage samples from Mycobacterium tuberculosis-infected mice. Bio Protoc
824 10:e3630.
825 82. Havenith CEG, Breedijk AJ, van Miert PPMC, Blijleven N, Calame W, Beelen
826 RHJ, Hoefsmit ECM. 1993. Separation of alveolar macrophages and dendritic
827 cells via autofluorescence: phenotypical and functional characterization. J Leukoc
828 Biol 53:504–510.
829 83. Banaiee N, Jacobs WR, Ernst JD. 2006. Regulation of Mycobacterium
830 tuberculosis whiB3 in the mouse lung and macrophages. Infect Immun 74:6449–
831 6457.
832 84. Srivastava S, Grace PS, Ernst JD. 2016. Antigen export reduces antigen
833 presentation and limits T cell control of M. tuberculosis. Cell Host Microbe 19:44–
834 54.
835 85. Layre E, Sweet L, Hong S, Madigan CA, Desjardins D, Young DC, Cheng TY,
836 Annand JW, Kim K, Shamputa IC, McConnell MJ, Debono CA, Behar SM,
837 Minnaard AJ, Murray M, Barry CE, Matsunaga I, Moody DB. 2011. A comparative

838 lipidomics platform for chemotaxonomic analysis of mycobacterium tuberculosis.
839 Chem Biol 18:1537–1549.
840 86. Safavi-Hemami H, Gajewiak J, Karanth S, Robinson SD, Ueberheide B, Douglass
841 AD, Schlegel A, Imperial JS, Watkins M, Bandyopadhyay PK, Yandell M, Li Q,
842 Purcell AW, Norton RS, Ellgaard L, Olivera BM. 2015. Specialized insulin is used
843 for chemical warfare by fish-hunting cone snails. PNAS USA 112:1743–1748.
844 87. Rgen Cox J, Hein MY, Luber CA, Paron I, Nagaraj N, Mann M. 2014. Accurate
845 proteome-wide label-free quantification by delayed normalization and maximal
846 peptide ratio extraction, termed MaxLFQ. Mol Cell Proteomics 13:2513–2526.
847

848 **Figure Legends**

849 **Figure 1. *M. tuberculosis* 4334 grows more rapidly but induces less cell**
850 **recruitment than H37Rv in early infection.** C57BL/6 mice were infected by aerosol
851 with 200-300 Colony Forming Units (CFU) of *M. tuberculosis* H37Rv, H37RvΔRD1
852 (ΔRD1), or 4334. Lungs were harvested at day 1, 3, 6, 8, 10, and 14 post-infection, and
853 processed to single cell suspensions. (**A**) Total CFU isolated from the lungs of mice
854 infected with the individual strains during the first 14 days of infection. (**B**) Total number
855 of cells isolated from the lungs of mice infected with the individual strains. Results are
856 shown as mean ± SD in 1(ΔRD1), 2 (4334), and 6 (H37Rv) pooled experiments, with
857 n=5 mice per strain per day in each experiment. Statistical significance was assessed
858 by multiple unpaired T-test for each day and Holm-Sidak multiple comparisons
859 correction, with a 95% confidence interval and *p<0.05, **p<0.01, ***p<0.001,

860 ****p<0.0001. For clarity, asterisks above H37Rv and 4334 are comparing only these 2
861 strains, and below are ΔRD1 compared to H37Rv.

862 **Figure 2. Differential strain-dependent spread of *M. tuberculosis* from**
863 **CD11b$^{neg/lo}$CD11c^{pos} alveolar macrophages to recruited lung myeloid cells.** Mice
864 were infected and lungs harvested as in Figure 1. (**A**) Cells were stained and analyzed
865 by flow cytometry for quantitation of CD11b$^{neg/lo}$CD11c^{pos} alveolar macrophages,
866 CD11b^{pos}CD11c^{pos} monocyte-derived dendritic cells, Gr-1^{hi}CD11c^{neg} neutrophils, Gr-
867 1^{int}CD11c^{neg} monocytes, and Gr-1^{neg}CD11c^{neg} monocyte-derived recruited macrophages
868 in the lungs (see Supplementary Figure 1 and Material and Methods for gating
869 strategy). (**B**) Total CFU in each leukocyte subset after live flow cytometry sorting and
870 plating of sorted cell populations on 7H11 solid media. Results are shown as mean ±
871 SD in 1 (ΔRD1), 2 (4334), and 6 (H37Rv) and pooled experiments, with n=5 mice per
872 strain per day in each experiment. Statistically significant difference between strains
873 was assessed multiple unpaired T-test for each day and Holm-Sidak multiple
874 comparisons correction, with a 95% confidence interval and *p<0.05, **p<0.01,
875 ***p<0.001, ****p<0.0001. For clarity, asterisks above H37Rv and 4334 are comparing
876 only these 2 strains, and below are ΔRD1 compared to H37Rv.

877 **Figure 3. *M. tuberculosis* strains 4334 and H37Rv do not produce PGL.** PGL and
878 PDIM analysis of *M. tuberculosis* H37Rv, HN878, and 4334 in 7H9 cultures, using
879 electrospray ionization-quadrupole time-of-flight-mass spectrometry (ESI-QTOF-MS).
880 Shown are representative images of (**A**) extracted ion chromatograms of PGL

881 [C114H212O18+NH4]+ at *m/z* 1887.601 and PDIM [C91H180O5+NH4]+ at *m/z*
882 1371.417, and (**B**) mass spectra. Strain HN878 was included in the analysis as a known
883 PGL producing positive control.

884 **Figure 4. *M. tuberculosis* strain 4334 replicates to a greater extent than H37Rv in**
885 **alveolar macrophages.** (**A**) Cultured alveolar macrophages were infected for 48 or 72h
886 with an MOI of 1 with *M. tuberculosis* H37Rv or 4334. Results are shown as mean CFU
887 fold-increase over initial inoculum. (**B**) Representative flow cytometry analysis of
888 cultured alveolar macrophages infected *in vitro* for 48h with *M. tuberculosis* H37Rv or
889 4334, each expressing DsRed fluorescent protein and stained with markers of necrosis
890 (Zombie Aqua, ZA) and apoptosis (Annexin V-APC). The upper panels show the
891 frequency of infected cells ($DsRed^+$) and lower panels staining with ZA and AV for cells
892 infected with the indicated strain 48h post-infection. (**C**) Percentage of $DsRed^+$ cultured
893 alveolar macrophages as quantitated from flow cytometry analysis using the gating
894 shown in panel B. (**D**) Frequency of cultured alveolar macrophages that are viable (ZA^-
895 AV^-), necrotic (ZA^+AV^-), early apoptotic (ZA^-AV^+) or late cell death (ZA^+AV^+) 48h after
896 infection with the indicated strain expressing DsRed fluorescent protein; bystanders are
897 defined as DsRed negative cells. Results are shown as mean ± SD for n=3 per time
898 point and per strain. Data between cells infected with respective strains were analyzed
899 by unpaired Student's t-test for each day and Holm multiple comparisons correction,
900 with a 95% confidence interval. Asterisks H37Rv vs 4334 (*$p<0.05$, **$p<0.01$,
901 ****$p<0.0001$), hashtag uninfected vs H37Rv or 4334 ($^{\#}p<0.05$, $^{\#\#}p<0.01$, $^{\#\#\#}p<0.001$).

902 **Figure 5. Earlier dissemination of *M. tuberculosis* strain 4334 to lymph nodes is**
903 **associated with a greater magnitude of Ag85B-specific CD4 T cell priming.** (**A**)

904 Bacterial load in mediastinal lymph nodes (MdLN) of mice infected 14 days earlier with
905 *M. tuberculosis* H37Rv or 4334. Results are shown as mean CFU fold-increase over
906 initial inoculum. Flow cytometry assessment (**B**) and absolute quantitation (**C**) of the
907 proliferation of CellTrace Violet-labeled adoptively transferred naïve P25TCR-
908 Tg/CD45.1 $CD4^+$ T cells in the MDLN 10-, 14-, and 17-days post-infection with H37Rv
909 or 4334. Percentages shown in panel B are the frequencies of adoptively transferred
910 P25TCR-Tg $CD4^+$ T cells in which CTV was diluted as a result of cell division (CTV^{dilute}).
911 Results in panel C are shown as mean ± SD, for n=4 mice per day and per strain. (**D**)
912 Quantitation of $IFN\gamma^+$ endogenous and P25TCR-Tg (as defined by congenic markers
913 CD45.1/2) $CD4^+$ T cells in the lungs of mice infected for 14 or 17 days with H37Rv or
914 4334. Results are shown as mean ± SD, for n=4 mice per day and per strain. Flow
915 cytometry analysis for these results is shown in Supplementary Figure 4B. Differences
916 between *M. tuberculosis* strains were assessed by Student's t-test for each day and
917 Holm multiple comparisons correction, with a 95% confidence interval and *$p<0.05$, and
918 **$p<0.01$.
919
920 **Supplemental Material Legends**
921 **Supplementary Figure 1. Flow cytometry gating strategy for identification of lung**
922 **myeloid cell populations**. After processing lung tissue into single-cell suspensions and
923 staining, cells were flow sorted first as $CD45^{neg}$ (non-hematopoietic) or $CD45^{pos}$. Further
924 cellular identification occurred using CD11b and CD11c to distinguish between **(1)**
925 $CD11b^{neg/lo}CD11c^{pos}$ alveolar macrophages and **(2)** $CD11b^{pos}CD11c^{pos}$ monocyte-
926 derived dendritic cells. Further differentiation of $CD11b^{pos}$ cells was done using CD11c

927 and Gr1, as **(3)** $Gr1^{hi}CD11c^{neg}$ neutrophils, **(4)** $Gr1^{int}CD11c^{neg}$ monocytes, and **(5)** Gr-
928 $1^{neg}CD11c^{neg}$ monocyte-derived recruited macrophages.

929 **Supplementary Figure 2. Strain-dependent spread of *M. tuberculosis* in recruited**
930 **myeloid cells.** (**A**) Cells were stained and analyzed by flow cytometry for quantitation of
931 subset and plated on 7H11 media (Figure 2). Depicted are the ratio of the average CFU
932 over the average cell number at each time point obtained post-infection in mice infected
933 with H37Rv, 4344, or ΔRD1. (**B**) Relative frequency of CFU recovered from myeloid cell
934 populations in the lungs of mice infected with *M. tuberculosis* H37Rv, ΔRD1, or 4334
935 after live flow sorting and plating of sorted cell fractions on 7H11 solid media. Results
936 are shown as mean ± SD in 1(ΔRD1), 2 (4334), and 6 (H37Rv) pooled experiments,
937 with n=5 mice per day and per strain in each experiment.

938 **Supplementary Figure 3. *M. tuberculosis* strains exhibit differential ESX-1 activity.**
939 H37Rv and 4334 were grown to logarithmic phase in 7H9, resuspended in Sauton's
940 media for 1 day, and filtrate proteins were reduced, alkylated, and trypsin digested prior
941 to run on LC-MS/MS. Spectra were searched against a combined database for H37Rv
942 and NITR203 on UniProt, using Andromeda search algorithm and MaxQuant for
943 quantitation. Statistical analysis done by Student t-test with Holm multiple comparisons
944 correction, 95% confidence interval, *$p<0.05$, and **$p<0.01$.

945 **Supplementary Figure 4. *M. tuberculosis* strain 4334 induces higher levels of IFNγ**
946 **in the lungs of mice than H37Rv after two weeks of infection.** (**A**) Total IFNγ levels
947 in the lung homogenate supernatants of mice infected with *M. tuberculosis* H37Rv or
948 4334. Results are shown as mean ± SD 4 experiments. Statistical significance was
949 assessed by unpaired Student's t-test for each day and Holm multiple comparisons

950 correction, with a 95% confidence interval and **p<0.01 and ***p<0.001. (**B**) Flow
951 cytometry gating strategy for the quantitation of IFNγ-producing $CD4^+$ T cells in the
952 lungs of mice infected with *M. tuberculosis* H37Rv or 4334 for 17 days.

953 **Supplementary Figure 5. *M. tuberculosis* strain 4334 induces a quantitatively**
954 **greater adaptive immune response compared to H37Rv that is sustained 7 weeks**
955 **after initial infection and results in more lesions in the lung.** Mice were aerosol
956 infected with 200-300 Colony Forming Units (CFU) of *M. tuberculosis* H37Rv or 4334
957 and harvested 7 weeks later. Lungs were processed to single cell suspensions and
958 plated on solid media for total CFU determination **(A)**, counted for total cell number **(B),**
959 and stained for flow cytometry analysis of cellular subsets **(D)** (see Supplementary
960 Figure 1 and Material and Methods for gating strategy). In addition, the left lung of
961 infected mice was fixed and stained with hematoxylin and eosin (H&E). **(C)** Using Fiji
962 open-source software, percentage of lung inflammatory infiltrate was calculated by
963 taking the total surface area of lung, subtracting contributions of airways and blood
964 vessels. Inflammatory infiltrates were quantitated by both manual contouring and
965 automated color density contouring, with the average of these values utilized for the
966 final percentage calculation. **(E)** Representative images of 5 μM sections at 40x (Leica
967 SCN400 F whole-slide scanner) are shown. Results are shown as mean ± SD of 4
968 mice. Statistical significance was assessed by unpaired Student's t-test and Holm
969 multiple comparisons correction with a 95% confidence interval and *p<0.05,
970 ***p<0.001, and ****p<0.0001.

971

Figure 1

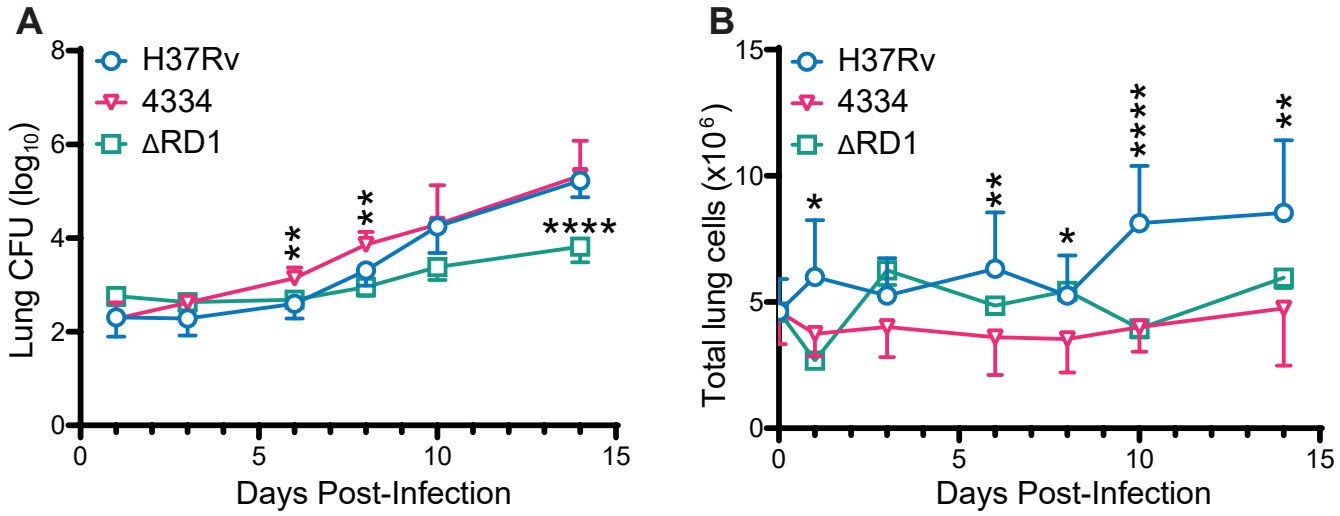
A
H37Rv
4334
ΔRD1
Lung CFU (log10)
Days Post-Infection
**
**
****
B
H37Rv
4334
ΔRD1
Total lung cells (x10^6)
Days Post-Infection
*
**
*
****
**

Figure 2

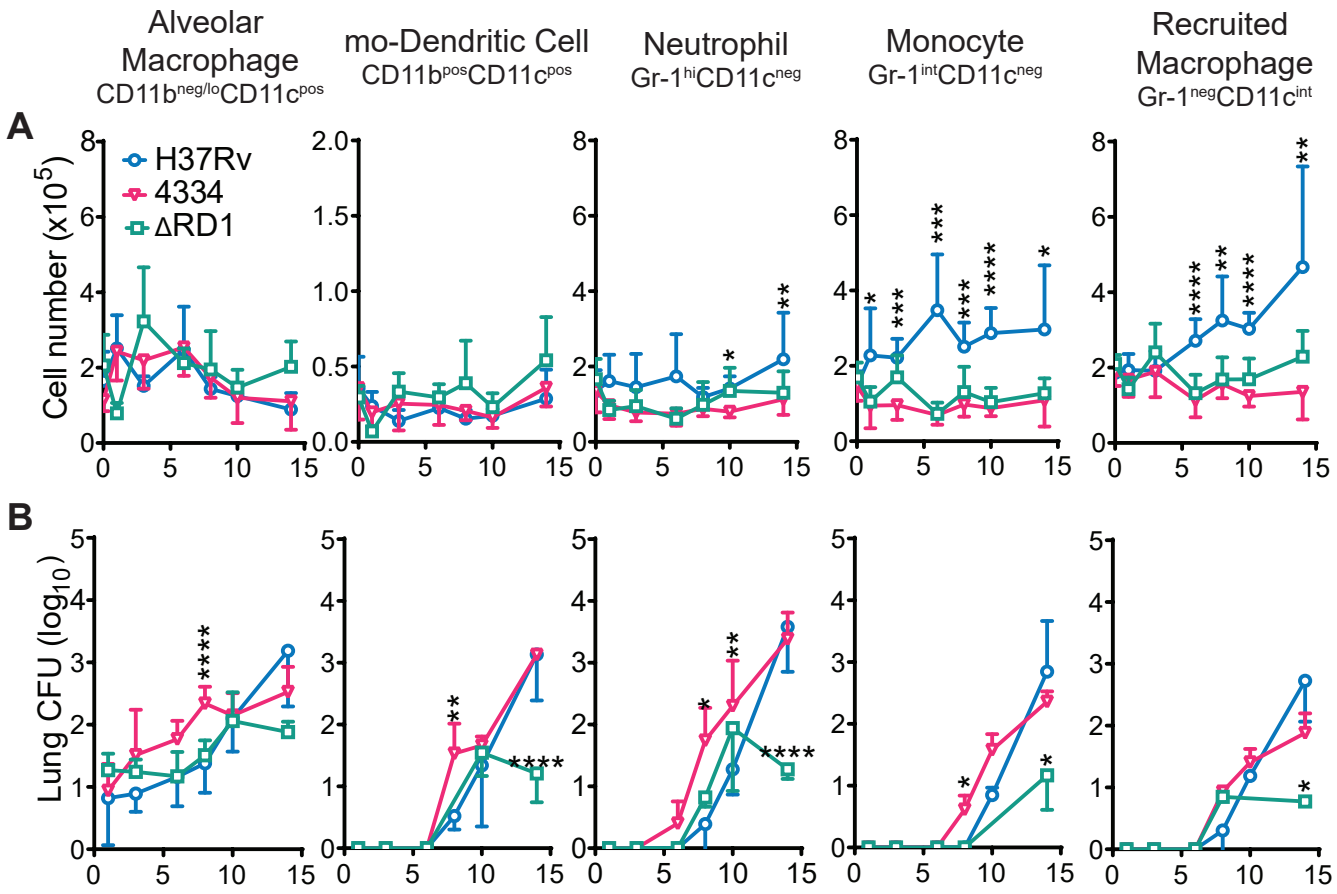
Alveolar Macrophage
CD11b$^{neg/lo}$CD11c^{pos}
mo-Dendritic Cell
CD11b^{pos}CD11c^{pos}
Neutrophil
Gr-1^{hi}CD11c^{neg}
Monocyte
Gr-1^{int}CD11c^{neg}
Recruited Macrophage
Gr-1^{neg}CD11c^{int}
A
B
H37Rv
4334
ΔRD1
Cell number (x10^5)
Lung CFU (log$_{10}$)

Figure 3

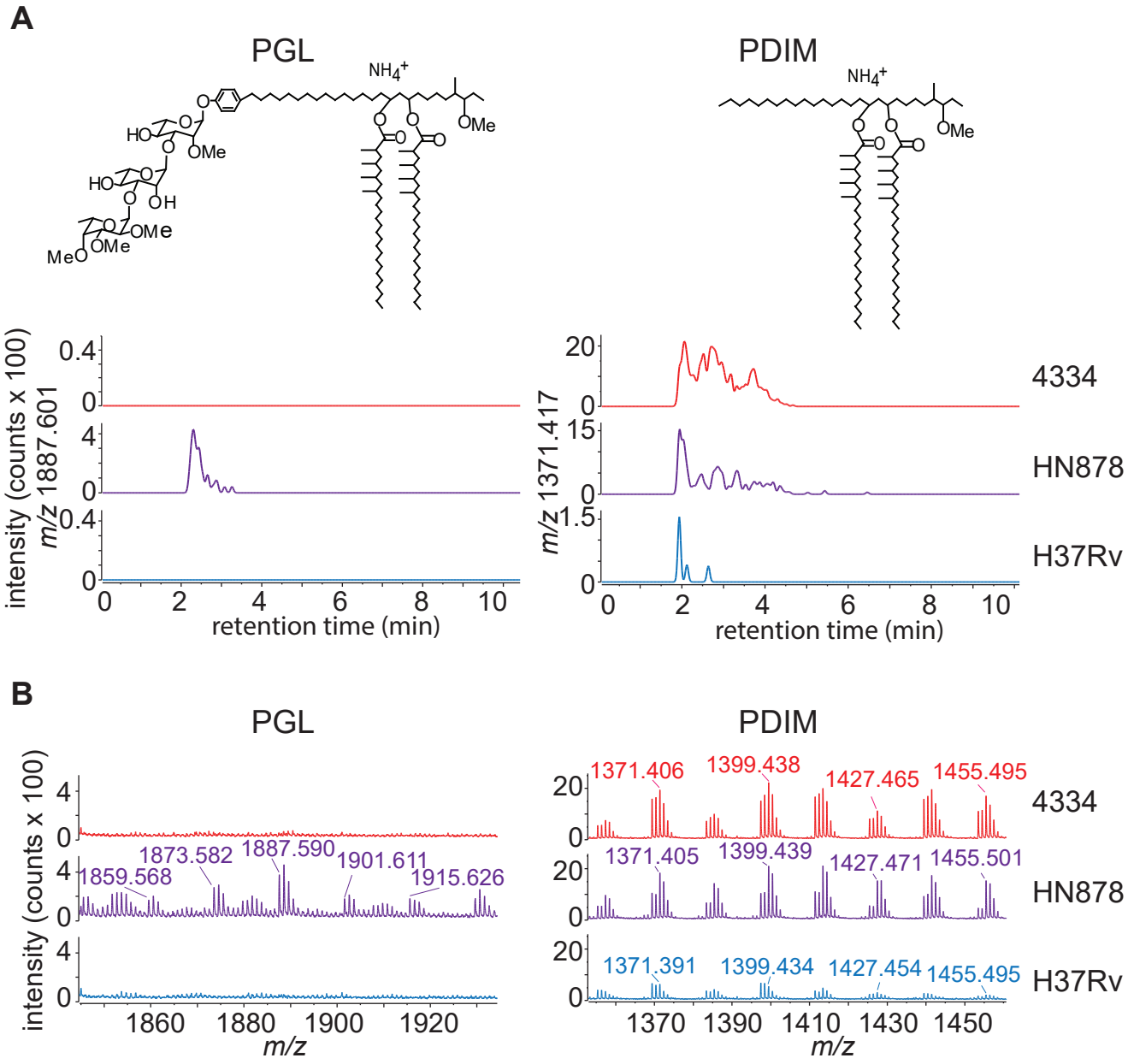
A
PGL
PDIM
NH4+
OMe
HO
OH
MeO
intensity (counts x 100)
m/z 1887.601
m/z 1371.417
retention time (min)
4334
HN878
H37Rv
B
1859.568
1873.582
1887.590
1901.611
1915.626
1371.406
1399.438
1427.465
1455.495
1371.405
1399.439
1427.471
1455.501
1371.391
1399.434
1427.454
1455.495
m/z

Figure 4

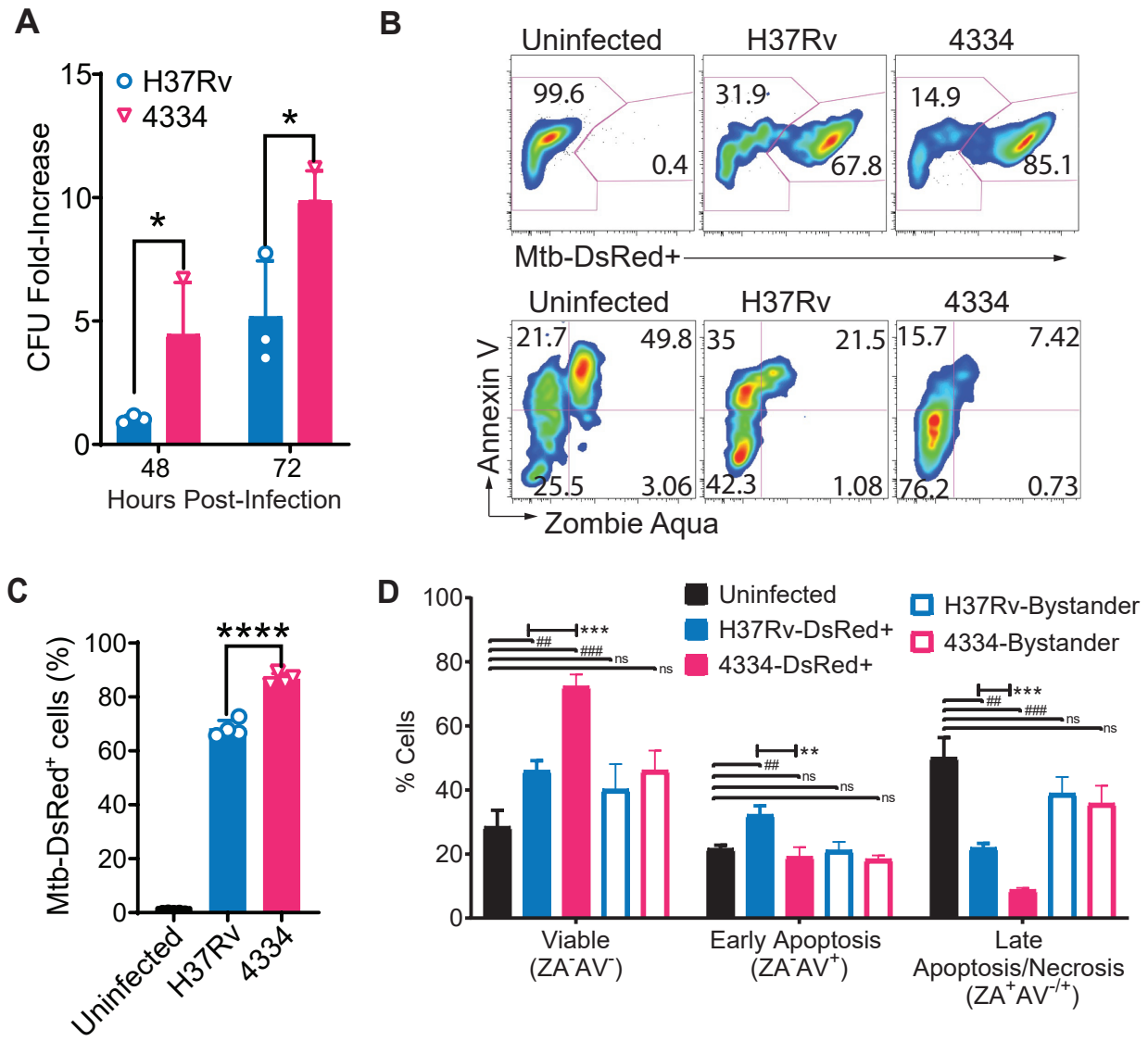
A
H37Rv
4334
CFU Fold-Increase
15
10
5
0
*
*
48
72
Hours Post-Infection
B
Uninfected
H37Rv
4334
99.6
0.4
31.9
67.8
14.9
85.1
Mtb-DsRed+
Uninfected
H37Rv
4334
Annexin V
21.7
49.8
25.5
3.06
35
21.5
42.3
1.08
15.7
7.42
76.2
0.73
Zombie Aqua
C
Mtb-DsRed+ cells (%)
100
80
60
40
20
0
****
Uninfected
H37Rv
4334
D
% Cells
100
80
60
40
20
0
Uninfected
H37Rv-DsRed+
4334-DsRed+
H37Rv-Bystander
4334-Bystander
***
##
###
ns
ns
**
##
ns
ns
ns
***
##
###
ns
ns
Viable
(ZA-AV-)
Early Apoptosis
(ZA-AV+)
Late
Apoptosis/Necrosis
(ZA+AV-/+)

Figure 5

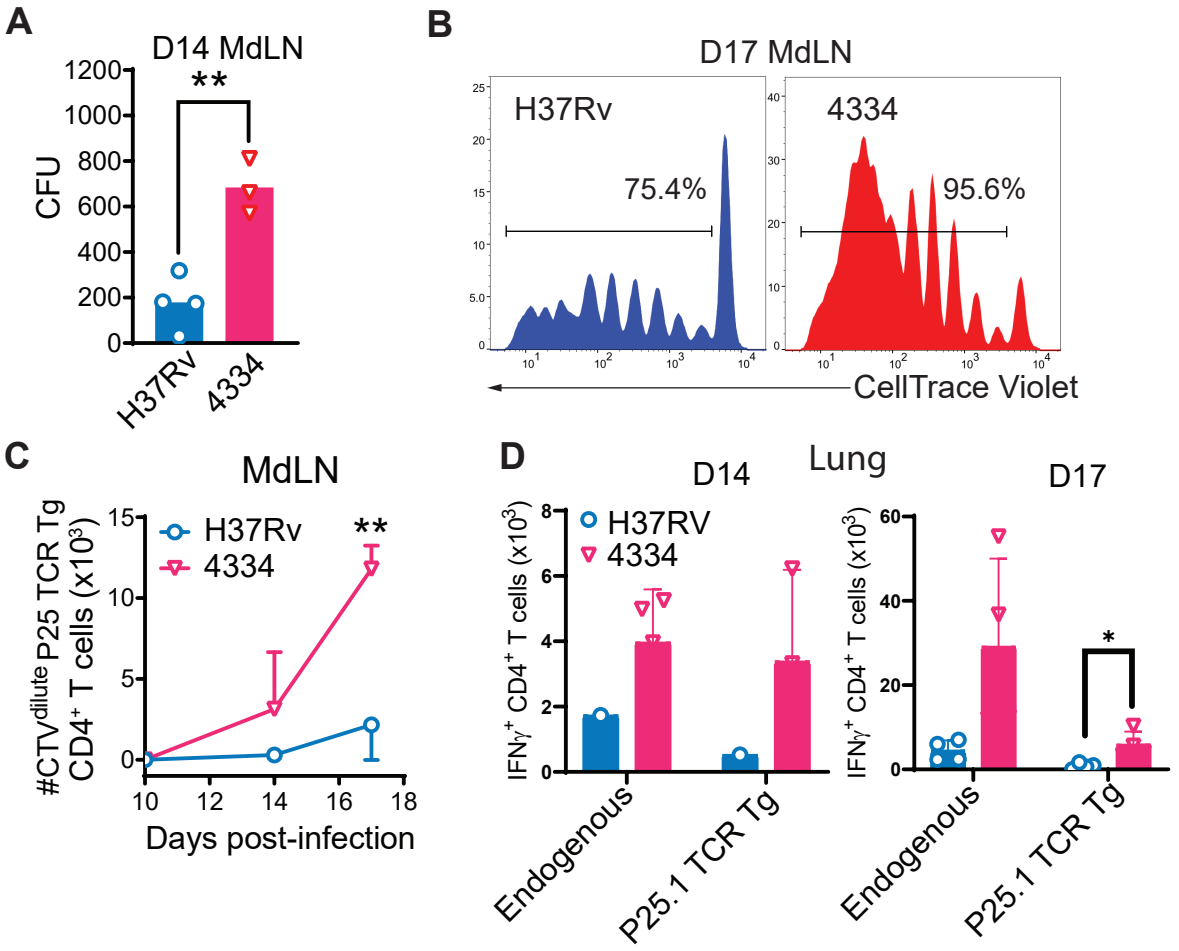
A
D14 MdLN
**
CFU
1200
1000
800
600
400
200
0
H37Rv
4334
B
D17 MdLN
H37Rv
75.4%
4334
95.6%
CellTrace Violet
C
MdLN
H37Rv
4334
**
#CTV^dilute P25 TCR Tg CD4+ T cells (x10^3)
Days post-infection
D
D14
Lung
D17
H37RV
4334
IFNγ+ CD4+ T cells (x10^3)
*
Endogenous
P25.1 TCR Tg